Journal of Materials Chemistry A

Accepted Manuscript

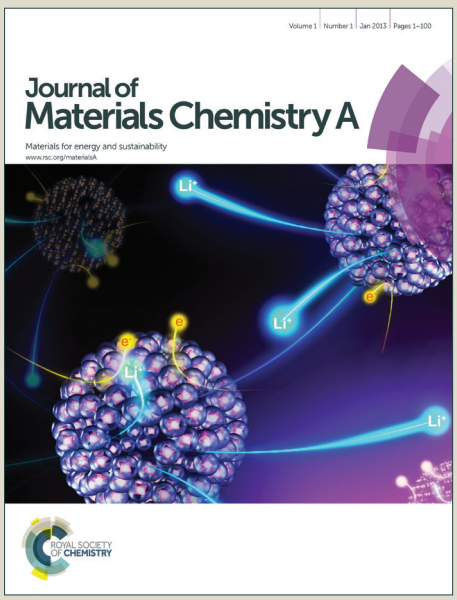

ROYAL SOCIETY OF CHEMISTRY

www.rsc.org/materialsA

Robust, Metallic $Pd_{17}Se_{15}$ and Pd_7Se_4 Phases From Single Source Precursor and Their Use as Counter Electrodes in Dye Sensitized Solar Cells

Suresh Kukunuri, S N Karthick and S. Sampath*
Department of Inorganic and Physical Chemistry
Indian Institute of Science
Bangalore 560012, India

Abstract

Thin films of conducting, palladium selenide phases ($Pd_{17}Se_{15}$ and Pd_7Se_4) are prepared using a single source molecular precursor by thermolysis. Varying the mole ratios of palladium and selenium precursors results in palladium organo-selenolate complexes which on thermolysis at different temperatures yield $Pd_{17}Se_{15}$ and Pd_7Se_4 phases that are very stable and adherent to the substrate. The organo-selenolate complexes are characterized using small angle XRD, ^{77}Se NMR and thermogravimetric analysis (TGA). The palladium selenide films are characterized by various techniques such as XRD, XPS, TEM and SEM. Electrical conductivities of the films are determined using four probe method. The strong adherence of the films to glass substrates coupled with high corrosion resistant behavior towards strong acid and alkaline environments render them to be very effective as electrocatalysts. The catalytic activity towards I_3^-/I^- redox couple, which is an important reaction in the regeneration of the dye in dye-sensitized solar cell is studied. Between the two phases, $Pd_{17}Se_{15}$ film shows superior activity as counter electrode for dye sensitized solar cells with photocurrent conversion efficiency of 7.45%.

1. Introduction

Metal chalcogenides based on platinum group elements have received enormous interest in recent years due to their unique properties leading to applications in catalysis, in semiconducting electronic devices, in lithographic and as optical discs and in organic molecular transformations.[1-4] Different types of chalcogenides such as binary, pseudo binary and ternary compounds with spinal structure are possible with platinum group metals. Palladium counterparts are also known to exist in several phases such as PdSe, $Pd_{17}Se_{15}$, Pd_7Se_4, $Pd_{2.5}Se$, Pd_3Se, Pd_4Se, $Pd_{4.5}Se$, Pd_7Se, Pd_8Se and $PdSe_2$.[5] The preparation procedure reported for these phases typically involves heating of the two constituent elements in an evacuated sealed quartz tube at high temperatures for several days.[5,6] There have been efforts directed towards fabricating thin films of chalcogenides using metal organic chemical vapour deposition (MOCVD) technique.[7-10] Among the palladium selenides, $Pd_{17}Se_{15}$ has received special attention due to its good thermal stability and superconducting behavior as in the case of $Rh_{17}S_{15}$.[11] Synthesis of $Pd_{17}Se_{15}$ using thermal decomposition of precursors based on metal organochalcogenato complexes has been recently reported. Jain et al. have reported the synthesis of palladium selenides by thermal decomposition of metal benzylselenolates, 2-(diethylamino)ethaneselenolates, monoselenocarboxylates and 2-(methoxycarbonyl)ethyl-selenolates complexes.[12-15] O'Brien et al. have used platinum and palladium dithio/ diselenoimidodiphosphinato complexes to synthesize metal selenides using low pressure chemical vapour deposition technique.[16,17] Singh et al. recently reported the synthesis of palladium selenides from selenoether complexes of palladium.[18,19] However, there is no report on the use of a single source precursor to synthesize different phases of palladium selenides. This will have an advantage since the composition can be controlled just by varying the precursor, metal salt ratio. The decomposition of the complexes would lead to

same by-products, if any. Hence, the variation in properties can be precisely attributed to varying composition of the metal selenides. Additionally, the electrical properties of palladium selenides are rarely reported.[11,20] The conducting phases may be useful as electrodes in electrochemical redox reactions as shown in the present study.

Dye-sensitized solar cells (DSSCs) have been attracting continuous attention of the scientific community since the time it was proposed a few decades ago. The solution based DSSCs have led to solid state devices and more recently to perovskite-based systems.[21,22] A DSSC consists of a photoanode with titanium dioxide adsorbed with a photosensitizing dye molecule, an electrolyte containing iodide/triiodide (I^-/I_3^-) redox couple, and a counter electrode. The counter electrode is an important element in the DSSC and very often fluorine doped tin oxide (FTO) glass coated with platinum is used. Recent studies have given rise to palladium-based electrodes,[23] carbon-based materials, nitrides etc.[24,25] The counter electrode stability and corrosion are issues of concern whether it is solution based DSSCs[26] or the more recently introduced system with Co-based electrolytes / perovskite based solar cells.[27]

In this direction, the present study reports the synthesis of different phases of palladium selenides namely, $Pd_{17}Se_{15}$ and Pd_7Se_4 by thermal decomposition method using a single precursor. Though the synthesis of certain phases of palladium selenides have been reported in the literature,[18] their use in electrocatalysis has not been well explored. Palladium is five times cheaper and relatively more abundant than platinum. When palladium combines with selenium, properties such as work function can vary. The amount of noble metal in the catalyst will decrease as well. In addition, there is no direct report on the synthesis of different phases based on single source precursors. The reaction of palladium salt with selenium precursors containing various mole ratios lead to different precursor complexes and subsequent decomposition in presence of nitrogen, yield single phase, uniform films with

good electrical conductivity. The films are characterized using electrical, microscopic and diffraction techniques before using them as counter electrodes in dye-sensitized solar cells.

2. Experimental

Palladium (II) acetate [$Pd(OAc)_2$], potassium selenocyanate (KSeCN), sodium borohydrate ($NaBH_4$) and 1-bromodecane were procured from Aldrich (USA) and were used without further purification. All organic solvents, toluene, N,N-dimethylformamide, acetone, ethanol, dichloromethane and iso-propanol were of AR grade and procured from polysales, India and used after standard purification / distillation procedures. The reaction involving selenium complex formation was monitored by ^{1}H, ^{13}C, and ^{77}Se NMR spectroscopy.

2.1 Synthesis of $Pd_{17}Se_{15}$ and Pd_7Se_4 phases

Palladium-organoselenolate complexes containing different compositions (Table 1) were prepared by mixing different mole ratios of palladium acetate and didecyl diselenide (DDDSe) (referred to as complex Axy where x and y correspond to the moles of $Pd(OAc)_2$ and the Se precursor) in toluene (2 mL). The resulting mixtures were stirred for 10 minutes at 25ºC. The selenium precursor DDDSe, was synthesized using a known procedure (complete synthesis and characterization of DDDSe is given in the SI).[28] The complexes were drop-casted on freshly cleaned glass slides of 1 cm^2 area. The films were allowed to dry and subsequently, the thermal decomposition of the complexes was carried out in a tubular furnace in presence of flowing N_2 at 250^{o}C for 1h. On thermal decomposition, the films turned to shiny black in color.

2.2 Characterization

The structure and morphology of the as-prepared palladium selenide films were obtained using X-ray diffraction (XRD) (PANalytical, Netherlands, Cu-K_α source), scanning electron microscopy (SEM) (Carl-Zeiss) and transmission electron microscopy (TEM, JEOL 2100F/FEI Tecnai 200 kV) techniques. The SEM was carried out on the as-prepared slide without any additional conducting coating and the samples for TEM studies was prepared by drop casting ethanol dispersions of the scratched material onto carbon coated copper/holey carbon grids. X-ray photoelectron spectroscopic analysis was performed on a Kratos Axis Ultra DLD X-ray photoelectron spectrometer with monochromatic Al kα excitation (1486.7 eV) radiation. The I-V measurements were carried out using four probe method on a Keithley 4200 work station. The thermogravimetric analysis (TGA) of the complexes was carried out in flowing argon atmosphere by using thermal analyzer, NETZSCH model TG 209 FI.

2.3 Components for electrochemical studies and solar cells

The counter electrode (CE) based on palladium selenide was prepared as follows. A layer of palladium-organoselenolate complex in toluene was drop casted on a conducting, transparent fluorine-doped tin oxide (FTO) surface. Different phases of palladium selenide films were prepared on FTO by varying the mole ratios of palladium and selenium precursors. Once the solvent evaporated, the complex was decomposed by heating the substrate at 250^oC for 1 hour in presence of flowing N_2 gas. The complex (red colour) turned into metallic palladium selenide phases with uniform thickness. The control experiment was carried out using Pt counter electrode prepared by the deposition of dilute Pt sol (Solaranix, Switzerland) in iso-propanol. A 15 μL aliquat of the sol was drop coated on FTO plate and kept on a hot plate, and subsequently heated to 450^oC, kept for 30 minutes and then cooled down to ambient conditions before further use.

The photoanode was prepared by using pre-cleaned FTO plates treated with 0.04 M of $TiCl_4$ solution for 30 minutes at ~ 80ºC. Subsequently, a 12 μm thick layer of 20 nm-sized TiO_2 particles was loaded on the modified surface (active area 0.25 cm^2). The plates were then heated by increasing the temperature slowly (75ºC over 10 minutes) and finally sintered at 450ºC for 30 minutes. The temperature was systematically decreased as earlier and finally maintained at 100ºC for few minutes to avoid moisture absorption. Two layers of TiO_2 were coated by following the same procedure. The plates were re-treated with $TiCl_4$ solution for 30 minutes and heated to 450ºC as given earlier. Once they are cooled to 100ºC, the plates were immediately soaked overnight in cis-di(isothiocyanato)-bis-(2,2'-bipyridal-4,4'-di-carboxylato)ruthenium(ll) bis-tetrabutylammonium (N719 dye, used as received from Solaronix SA, Switzerland) solution (0.3 mM in a mixed solvent of acetonitrile and tert-butanol in the ratio of 1:1 by volume) and used for fabricating the cell.

A solution of 0.1 M lithium iodide (LiI), 0.05 M I_2 in 10 mL of dry acetonitrile was prepared along with 0.6 M 1,2-dimethyl-n-propylimidazolium iodide, and 0.5 M 4-tert-butylpyridine and used as the electrolyte for DSSCs. All the preparations were carried out in glove box. The dye-sensitized TiO_2 photoanode and the CE were separated by a hot-melt surlyn polymer film (60 μm thick) and sealed through hot-pressing. The redox electrolyte was injected into the inter space between the photoanode and CE. Finally, the holes on the back of the CE were sealed with the polymer covered with a thin glass slide under heat.

2.4 Electrochemical studies

Cyclic voltammetry (CV) was carried out in a three-electrode system containing anhydrous acetonitrile solution of 0.1 M $LiClO_4$, 10 mM LiI and 1 mM I_2 at different scan rates, using a large Pt wire as the counter electrode, Ag/Ag^+ electrode as the reference electrode, and the as-prepared palladium selenide films as the working electrode. Symmetric cells with two identical palladium selenide electrodes separated by the electrolyte were used

for electrochemical impedance spectroscopy (EIS) and polarization measurements. The active area used was 0.25 cm^2. The samples were scanned from 0.01 Hz to 1 MHz at 0 V bias with ac amplitude of 10 mV for impedance measurements. The photocurrent density- photovoltage curves of DSSCs were recorded on Keithley 2400 source meter under the illumination of AM1.5 solar light from a solar simulator equipped with Xe lamp (300 W). The light intensity was calibrated using a reference Si solar cell.

3. Results and discussion

The palladium selenide films formed on different substrates such as glass and FTO are very stable and adherent. The thicknesses of the coatings vary from 2 to 8 μm depending on the volume of precursor solution used. The crystalline nature of the as-formed palladium decylselenolate complex (A11) coated on a glass substrate is characterized using x-ray diffraction. Sharp diffraction peaks observed in the XRD pattern [Fig. 1(a)] corresponds to d-spacings of 29.06, 14.37, and 9.56 Å, which can be assigned to the (001), (002), and (003) reflections respectively. The (001) reflection is a direct measure of the bilayer thickness as reported in the case of palladium dodecane-thiolate.[29] The d-spacing values obtained in the case of decylselenolate is less than that of the value observed for dodecanethiolate (d-spacing value for (001) plane is 40 Å) and may be attributed to the absence of two methylene groups as well as orientation changes (each methylene group corresponds to 2.48 Å). The precursor formed is a 1:1 complex of formula, $Pd(SeR)_2$. The ^{77}Se NMR signal for the complex A11 shifts by 70 ppm to the shielded region as compared to the free ligand (i.e.) RSeSeR (Fig. S1). This observation is similar to that observed for palladium selenoether complexes.[18] The thermogravimetric analysis of complex A11 (11 corresponds to the molar ratio of $Pd(OAc)_2$ to RSeSeR of 1:1) carried out under flowing argon atmosphere [Fig. 1(b)] shows that the decomposition occurs in two steps. The first small loss is due to elimination of solvent and

next reduction in mass is due to the removal of alkyl chains present in the complex to form the palladium selenide of composition, $Pd_{17}Se_{15}$. The second, large weight loss is in agreement with the calculated weight loss for the complex $[Pd(SeR)_2]$ decomposition to form $Pd_{17}Se_{15}$ at a temperature of 250^{o}C. The TGA analysis carried out for the decomposition of complex A41 (41 corresponds to the molar ratio of $Pd(OAc)_2$ to RSeSeR of 4:1) shows a major weight loss of ~ 45 % (Fig. S2) in the temperature range of 150 - 200°C. The characterization of the complex (A41) by XRD reveals that the pattern is dominated by intense $Pd(OAc)_2$ diffraction peaks. Additionally, the weight loss to form Pd_7Se_4 does not correspond to the complex as in the previous case of A11 $[Pd(SeR)_2]$. On the contrary, the calculated weight loss with the complex of composition Pd(SeR)(OAc) is in agreement with the experimental weight loss data. Further studies are required to understand the nature of the complex. Since the preparation conditions for the two palladium selenide phases are optimized and highly reproducible, we have continued with the procedure for synthesis and used the selenides for further studies.

The XRD pattern of $Pd_{17}Se_{15}$ [Fig. 2(a)] reveals cubic phase with lattice parameter, a = 10.06 Å and the pattern matches with the literature data (JCPDF 73-1424). The crystallite size as determined using Scherrer formula is ~ 102 nm. Thermal decomposition of the complex A11 has been followed by *in-situ* XRD at different temperatures. Figure 2b shows the *in-situ* XRD patterns and it is observed that the diffraction peaks corresponding to $Pd_{17}Se_{15}$ phase start to appear at temperatures ~ 200^{o}C. This indicates that the thermal decomposition of complex A11 ~ 250^{o}C is sufficient to form pure $Pd_{17}Se_{15}$ phase. The XRD pattern observed for Pd_7Se_4 corresponds to orthorhombic system with lattice parameters, a = 5.23, b = 6.87 and c = 6.21 Å (JCPDF 31-0939). The crystallite size determined using Scherrer formula is ~ 76 nm. Transition of composition from $Pd_{17}Se_{15}$ to Pd_7Se_4 is observed

when the mole ratio of the complex A is varied from 1:1 to 4:1 and the end-materials are phase-pure [Fig. 2(c)]. The XRD patterns of the products formed from complexes with intermediate molar ratios, A21 and A31 show the presence of peaks corresponding to both $Pd_{17}Se_{15}$ and Pd_7Se_4 phases [Fig. S3(a)].

When complexes formed from $Pd(OAc)_2$:RSeSeR wherein Se precursor content is higher than that of palladium precursor, (with molar ratios of 1:2, 1:3 and 1:4) are decomposed, a new phase $PdSe_2$ [Fig. 2(d)] along with $Pd_{17}Se_{15}$ is observed [Fig. S3(b)]. The formation of $PdSe_2$ phase is confirmed by the presence of diffraction peak at 23° corresponding to the (002) plane, which is absent in the case of $Pd_{17}Se_{15}$ phase [Fig. 2(a)]. Table 1 shows the summary of phases formed with different mole ratios of a palladium organoselenolate complex.

The $Pd_{17}Se_{15}$ and Pd_7Se_4 phases are found to be very stable in highly acidic (1 M H_2SO_4) and alkaline (6 M KOH) environment without any change composition (based on XRD patterns after immersion for 24 h, Fig. S4). The electrical properties of the two selenide phases reveal that they possess metallic conductivity and hence can be employed in electrochemical cells as electrodes. This is particularly important in applications in areas such as fuel cells and water splitting where harsh acidic and alkaline conditions are employed. Thermal stability of $Pd_{17}Se_{15}$ phase is tested by heating the film in ambient atmosphere (Fig. S5) and it is found that the pure phases are retained up to 400°C.

The elemental composition and the chemical state are characterized by X-ray photoelectron spectroscopy. The spectra of Pd-3d region of the two phases ($Pd_{17}Se_{15}$ and Pd_7Se_4) are compared with that observed for Pd (0) prepared under identical conditions by the decomposition of $Pd(OAc)_2$. Table 2 shows the binding energy values of Pd and Se in the two phases. A spin-orbit separation of 5.2 eV is observed for Pd-3d signal in both $Pd_{17}Se_{15}$ and

Pd_7Se_4 phases. The palladium $3d_{5/2}$ and $3d_{3/2}$ peaks for $Pd_{17}Se_{15}$, are observed at 336.2 eV and 341.5 eV respectively [Fig. 3(a)]. These values lie in between those observed for Pd in PdS and PdTe.[30,31] The peaks corresponding to selenium, $3d_{5/2}$ and $3d_{3/2}$ are observed at 54.4 and 55.2 eV respectively [Fig. 3(b)]. Here again, there is a shift ($3d_{5/2}$ and $3d_{3/2}$) observed towards lower binding energies as compared to Se (0), indicating that selenium in $Pd_{17}Se_{15}$ and Pd_7Se_4 phases possesses negative charge which is quite common in metal selenides phases.[32-35] It should also be pointed out that the Pd peaks shift towards Pd (0) values when the Pd content in the palladium selenide phase is increased (from $Pd_{17}Se_{15}$ to Pd_7Se_4).[36,37]

The surface morphology of the palladium selenide films is assessed using field emission scanning electron microscopy (FESEM). The morphology of $Pd_{17}Se_{15}$ on FTO glass shows that the film is continuous with uniform porous structure, and the pore size distribution is highly reproducible. In the case of Pd_7Se_4, the morphology shows both micro- and macro pores with certain discontinuity (Fig. 4). The morphology of Pd_7Se_4 depends on the volume of the precursor used for thermolysis. The morphologies being different may affect the electrocatalytic properties and in turn the DSSC characteristics. The energy dispersive x-ray analysis (EDX) of the phases shows the presence of palladium and selenium, along with small amount of carbon (Fig. S6). The presence of carbon is likely to be due to the decomposition of alkyl chains in the palladium organoselenolate complex. The palladium to selenium ratios from EDX analysis match with the corresponding phases based on the XRD studies. Figure 5 shows the transmission electron microscopy (TEM) images of the two phases ($Pd_{17}Se_{15}$ and Pd_7Se_4). Interplanar distances based on high resolution TEM (HRTEM) are found to be 3.19 and 2.68 Å for $Pd_{17}Se_{15}$ and Pd_7Se_4 phases respectively. This corresponds to (113) and (311) planes of $Pd_{17}Se_{15}$ and Pd_7Se_4.[17] The selected area electron diffraction (SAED) patterns [Fig. 5(c-d)] show discrete spots indicating good crystallinity of

the materials and the interpretation of all the rings are shown in the corresponding figures. Raman spectra of $Pd_{17}Se_{15}$ and Pd_7Se_4 are presented in figure 6 and the studies reveal bands at 146, 208, 224 and 260 cm^{-1} corresponding to $Pd_{17}Se_{15}$ [Fig. 6(a)]. $Pd_{17}Se_{15}$ is isostructural with $Rh_{17}S_{15}$ and the vibrational bands are expected to be similar.[38] Weak bands observed at 1381 and 1588 cm^{-1} reveal the presence of very small amount of carbon in the material in the case of $Pd_{17}Se_{15}$ while the intensities for D and G bands of carbon in the case of Pd_7Se_4 are large, possibly due to the presence of large amount of the Se precursor. The thickness of the films measured using optical surface profilometer show values of 2.3 μm and 7.5 μm for $Pd_{17}Se_{15}$ and Pd_7Se_4 respectively (Fig. 7, S7) and are uniform across the substrate. The thickness of the films varies with amount of complex used for thermal decomposition.

Electrical measurements are carried out using four probe van der Pauw method wherein the films are given contacts to four probes using silver dots at four corners. The electrical resistivity of $Pd_{17}Se_{15}$ at 25°C is calculated to be 29 μΩ cm. This value matches with that of the reported value in the literature wherein the $Pd_{17}Se_{15}$ is prepared by reacting the elements in evacuated quartz tube at high temperatures.[11,20] Hence, the contribution by the remnant carbon in the thermally decomposed film is minimum. In the case of Pd_7Se_4, the electrical resistivity values are found to be 50.17 μΩ cm at 25°C. The temperature dependent resistivity measurements on Pd_7Se_4 (Figure 7) indicate that the phase is metallic in nature. The $Pd_{17}Se_{15}$ phase has already been reported to possess metallic conductivity [(20)] (Fig. S7).

Electrochemical studies:

The $Pd_{17}Se_{15}$ and Pd_7Se_4 phases are electrically conducting in nature and are highly stable in harsh electrolyte conditions. Hence, they may be very useful as electrodes to drive redox reactions. This aspect of palladium selenides has not been, hitherto, explored and the present study demonstrates their use in dye sensitized solar cells (DSSCs). In DSSC, Pt is

generally used as counter electrode. Efforts are underway to find alternate electrode materials[39-42] since Pt is known to undergo corrosion in presence of I_3^-/I^- couple.[43] The role of counter electrode in DSSC is to reversibly carry out the redox reaction involving I_3^-/I^- couple.

In order to study the electrocatalytic activity of the two phases towards the I_3^-/I^- redox couple, cyclic voltammetry, electrochemical impedance and Tafel polarization are carried out in a two electrode set-up in acetonitrile containing 0.1M $LiClO_4$ and I_3^-/I^-. The voltammogram observed on a Pt electrode reveals two redox pairs [Fig. 8(b)] which correspond to the reactions given in below. The efficiency of a DSSC depends on the regeneration of the dye which in turn depends on the regeneration of I^- ions in the electrochemical cell. Therefore, the kinetics of the redox reactions assumes importance.

$$I_3^- + 2e^- \longleftrightarrow 3I^- \qquad (1)$$

$$I_2 + 2e^- \longleftrightarrow 2I_3^- \qquad (2)$$

In the case of $Pd_{17}Se_{15}$, the difference in peak potentials of the cathodic and anodic processes, ΔE_p of the first redox pair is observed to be 250 mV whereas for Pd_7Se_4, the reduction peak of the first redox couple is not prominently observed [Fig. 8(b)]. This behavior is reported to be observed in carboneous, titanium-based materials and some metal chalcogenides such as NiSe, CoSe.[44] From the observed ΔE_p values, $Pd_{17}Se_{15}$ seems to possess better electrocatalytic activity than that of Pd_7Se_4. Figure 8(c) shows the Tafel polarization curves of the two phases, which are recorded in a symmetrical cell. The Tafel slopes observed for $Pd_{17}Se_{15}$ is comparable to that observed on Pt where the kinetics of the redox reaction is reported to be good. The Tafel slope observed in the case of Pd_7Se_4 is lower than that observed on $Pd_{17}Se_{15}$. The exchange current densities (J_0) which are the direct measure of electrochemical kinetics are calculated based on polarization curves and are found

to be higher for $Pd_{17}Se_{15}$ (11.5 mA/cm^2) than that of Pd_7Se_4 (9.5 mA/cm^2) while the value is 13.5 mA/cm^2 for Pt (Fig. S8).

Electrochemical impedance data in the Nyquist form are shown in figure 8(d) for $Pd_{17}Se_{15}$, Pd_7Se_4 and Pt. Two semi circles are observed and the one in the high frequency region is due to charge transfer resistance, double layer capacitance and Warburg diffusion (Z_w) at the electrode / electrolyte interface. The right semi circle in the low frequency region is attributed to the Nernst diffusion impedance (Z_N) of the redox couple in the electrolyte.[45,46] The equivalent circuit which is obtained by fitting the corresponding data points is shown in the inset of figure 8 (d). The parameters such as R_s, R_{ct}, C_{dl} and Z_w obtained for the two phases are given in table 3. The charge transfer resistance is observed to be lower for $Pd_{17}Se_{15}$ than that observed for Pd_7Se_4 indicating better electrocatalytic activity for the $Pd_{17}Se_{15}$ phase. Work function measurements for the two phases (Fig. S9) along with palladium prepared from the same precursor by thermal decomposition of $Pd(OAc)_2$ reveal values of 4.6 ± 0.1, 4.4 ± 0.1, 4 ± 0.1 eV corresponding to $Pd_{17}Se_{15}$, Pd_7Se_4 and Pd. The observed work function value for Pd is less than value observed for commercial Pd and is attributed due to the remnant carbon present along with Pd.[47]

Figure 8(a) depicts the solar cell characteristics of photocurrent versus photovoltage plot and the performance characteristics are summarized in table 3. The short circuit photocurrent densities are found to be high, and close to that observed for DSSC with Pt counter electrodes (16 mA/cm^2). As observed, the fill factor is higher for $Pd_{17}Se_{15}$ than that of Pd_7Se_4 and this reflects in the overall conversion efficiency being 7.45 % for $Pd_{17}Se_{15}$ while it is 6.88 % for Pd_7Se_4 as counter electrode. The efficiency is comparable to that observed on a Pt counter electrode under identical conditions. The difference in morphologies of the $Pd_{17}Se_{15}$ and Pd_7Se_4 may possibly play a role in their DSSC characteristics being different.

4. Summary

In summary, a simple thermolysis based on single source molecular precursor is employed for the synthesis of thin films of stable palladium rich selenide phases such as $Pd_{17}Se_{15}$ and Pd_7Se_4, by varying the mole ratio of palladium and selenium precursors. The two phases show very good stability in highly acidic and alkaline environment thus offering themselves as good candidates for electrcatalysis. Solar conversion efficiencies of 7.45% and 6.88% are obtained for $Pd_{17}Se_{15}$ and Pd_7Se_4 films as compared to standard Pt based electrodes (7.61%). The favourable electrochemical properties based on electrochemical impedance parameters point out that there is scope for improvement towards other electrochemical reactions such as hydrogen evolution and oxygen reduction that are being studied.

5. Acknowledgement: The authors thank DST, New Delhi for financial support under the US-India Partnership to Advance Clean Energy-Research (PACER) for the Solar Energy Research Institute for India and the United States (SERIIUS).

References

1 S. Dey, V. K. Jain, *Platinum Met. Rev.,* 2004**, 48**, 16-29.

2 L. Y. Chiang, J. W. Swirczewski, R. Kastrup, C. S. Hsu and R. B. Upasani, *J. Am. Chem. Soc.,* 1991**, 113**, 6574-6584.

3 S. Eijsbouts, V. H. J. DeBeer and R. Prins, *J. Catal.,* 1988**, 109**, 217-220.

4 Y. Min, G. D. Moon, C.-E. Kim, J.-H. Lee, H. Yang, A. Soon and U. Jeong, *J. Mater. Chem. C,* 2014, **2**, 6222–6248.

5 T. Olsen, E. Rost and F. Gronvold, *Acta Chem. Scand. A*, 1979, **33**, 251-256.

6 S. Geller, *Acta Crystallogr.*, 1962, **15**, 713-721.

7 A. L. Abdelhady, M. Afzaal, M. A. Malik and P. O'Brien, *J. Mater. Chem.*, 2011, **21**, 18768–18775.

8 M. Afzaal, C. L. Rosenberg, M. A. Malik, A. J. P. White and P. O'Brien, *New J. Chem.*, 2011, **35**, 2773–2780.

9 J. Akhtar, M. Afzaal, M. A. Vincent, N. A. Burton, I. H. Hillier and P. O'Brien, *Chem. Commun.*, 2011, **47**, 1991-1993.

10 J. Akhtar, M. Afzaal, M. A. Vincent, N. A. Burton, J. Raftery, I. H. Hillier and P. O'Brien, *J. Phys. Chem. C*, 2011, **115**, 16904-16909.

11 H. R. Naren, A. Tamizhavel and S. Ramakrishan, *Journal of Physics: Conference Series*, 2011, **273**, 012074.

12 S. Dey, V. K. Jain and B. Varghese, *J. Organomet. Chem.*, 2001, **623**, 48-55.

13 M. K. Pal, V. K. Jain, N. P. Kushwah, A. Wadawale, S. A. Glazun, Z. A. Starikova and V. I. Bregadze, *J. Organomet. Chem.*, 2010, **695**, 2629-2634.

14 L. B. Kumbhare, V. K. Jain, P. P. Phadnis and M. Nethaji, *J. Organomet. Chem.*, 2007, **692**, 1546-1556.

15 L. B. Kumbhare, V. K. Jain and B. Varghese, *Inorg. Chim. Acta*, 2006, **359**, 409-416.

16 P. L. Musetha, N. Revaprasadu, G. A. Kolawole, R. V. S. R. Pullabhotla, K. Ramasamy and P. O'Brien, *Thin Solid Films*, 2010, **519**, 197.

17 J. Akhtar, R. F. Mehmood, M. A. Malik, N. Iqbal, P. O'Brien and J. Raftery, *Chem. Commun.*, 2011, **47**, 1899-1901.

18 V. V. Singh, G. K. Rao, A. Kumar and A. K. Singh, *Dalton Trans*, 2012, **41**, 1142.

19 H. Joshi, K. N. Sharma, A. K. Sharma, Om Prakash and A. K. Singh, *Chem. Commun.,* 2013, **49**, 7483.

20 A. Kjekshus, *Acta. Chem. Scand*, 1973, **27**, 4.

21 J. Burschka, N. Pellet, S.-J. Moon, R. H. Baker, P. Gao, M. K. Nazeeruddin and M. Gratzel, *Nature*, 2013, **499**, 316.

22 H. J. Snaith, *J. Phys. Chem. Lett.*, 2013, **4**, 3623–3630.

23 N. A. M. Barakat, M. S. Akhtar, A. Yousef, M. El-Newehy and H. Y. Kim, *Chem. Eng. J.*, 2012, **211**, 9–15.

24 G. R. Li, F. Wang, Q. W. Jiang, X. P. Gao and P. W. Shen, *Angew. Chem., Int. Ed.*, 2010, **49**, 3653–3656.

25 M. Wu, H. Guo, Y. Lin, K. Wu, T. Ma and A. Hagfeldt, *J. Phys. Chem. C*, 2014, **118**, 12625.

26 S. Altobello, R. Argazzi, S. Caramori, C. Contado, S. D. Fre, P. Rubino, C. Chone, G. Larramona and C. A. Bignozzi, *J. Am. Chem. Soc.*, 2005, **127**, 15342–15343.

27 M. R. Narayan, *Renewable and Sustainable Energy Reviews*, 2012, **16**, 208–215.

28 J. Muller and A. Terfort, *Inorg. Chim. Acta*, 2006, **359**, 4821-4827.

29 N.S. John, P. J. Thomas and G. U. Kulkarni, *J. Phys. Chem. B*, 2003, **107**, 11376.

30 A. B. Volynski, A. Yu. Stakheev, N. S. Telegina, V. G. Senin, L. M. Kustov and R. Wennrich, *Spectrochim. Acta, Part B,* 2001, **56**, 1387–1396.

31 S. B. Elvy, P. A. Williams and A. N. Buckley, *Surf. Interface Anal.,* 1996, **24**, 641–646.

32 W. D. Shi, X. Zhang and G. B. Che, *Int. J. Hydrogen Energy,* 2013, **38**, 7037-7045.

33 X. Chen and R. Fan, *Chem. Mater.*, 2001, **13**, 802-805.

34 Y. Zhang, Z. Qiao and X. Chen, *J. Mater. Chem.,* 2002, **12**, 2747.

35 Y. Xie, X. W. Zheng, X. C. Jiang, J. Lu and L. Y. Zhu, *Inorg. Chem.*, 2002, **41**, 387–392.

36 J. Zhang, Y. Xu and B. Zhang, *Chem. Commun.*, 2014, **50**, 13451-13453.

37 V. V. Singh, U. Kumar, S. N. Tripathi and A. K. Singh, *Dalton Trans.*, 2014, **43**, 12555–12563.

38 N. Singh, J. Hiller, H. Metiu and E. McFarland, *Electrochim. Acta*, 2014, **145**, 224–230.

39 Y. Xiao, G. Han, Y. Li, M. Li and J. Y. Lin, *J. Power Sources,* 2015, **278**, 149-155.

40 H. Ma, J. Tian, S. Bai, X. Liu and Z. Shan, *Electrochim. Acta*, 2014, **137**, 138-145.

41 J. Wu, Y. Xiao, Q. Tang, G. Yue, J. Lin, M. Huang, Y. Huang, L. Fan, Z. Lan, S. Yin and T. Sato, *Adv. Mater.*, 2012, **24**, 1884–1888.

42 Q. W. Tang, H. Y. Cai, S. S. Yuan and X. Wang, *J. Mater. Chem. A*, 2013, **1**, 317–323.

43 G. Syrrokostas, A. Siokou, G. Leftheriotis, P. Yianoulis, 2012, **103,** 119-127.

44 F. Gong, H. Wang, X. Xu, G. Zhou and Z. S. Wang, *J. Am. Chem. Soc.*, 2012, **134**, 10953–10958.

45 L. Wang, Y. Shi, X. Bai, Y. Xing, H. Zhang, L. Wang, W. Guo, N. Wang, T. Ma and M. Grätzel, *Energy Environ. Sci.*, 2014, **7**, 343–346.

46 X. J. Zheng, J. H. Guo, Y. T. Shi, F. Q. Xiong, W. H. Zhang, T. L. Ma and C. Li, *Chem. Commun.*, 2013, **49**, 9645.

47 R. Bhatt, S. Bhattacharya, R. Basu, A. Singh, U. Deshpande, C. Surger, S. Basu, D. K. Aswal and S. K. Gupta, *Thin Solid Films,* 2013, **539**, 41.

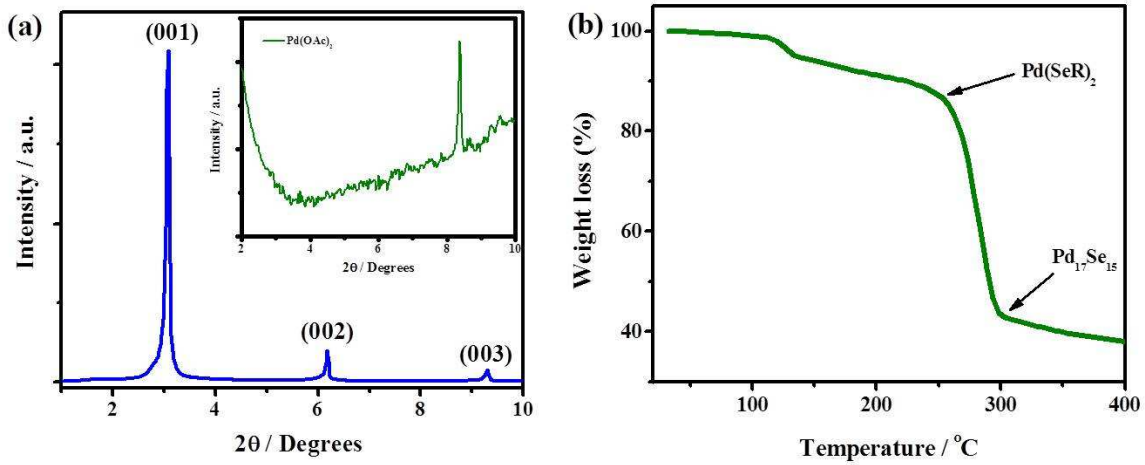

Figure 1. (a) XRD pattern of palladium decylselenolate complex (A11) coated on glass slide. [Inset shows the XRD of only $Pd(OAc)_2$ on glass slide] and (b) Thermo gravimetric (TG) curve carried out on the same complex in presence of flowing argon at a temperature rate of 10º C/min.

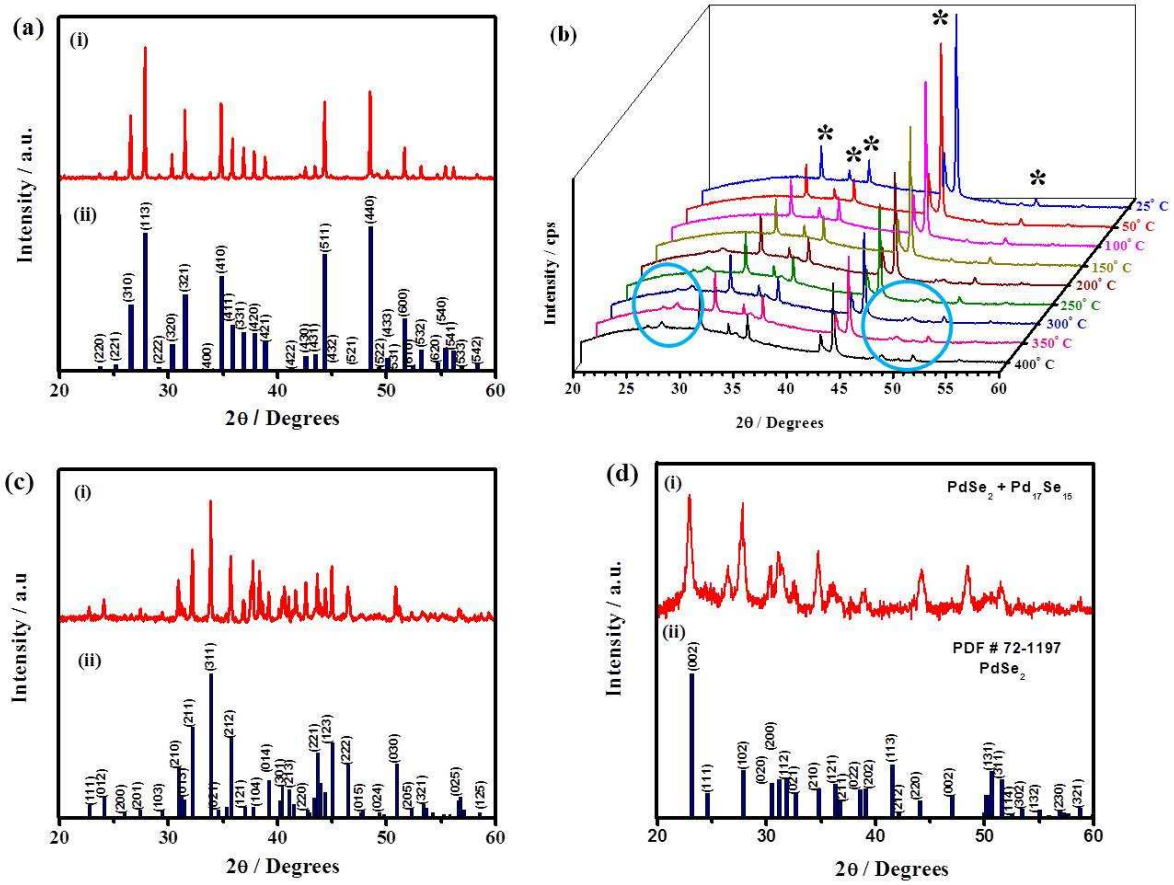

Figure 2. (a) XRD patterns of thin films of (i) $Pd_{17}Se_{15,}$ obtained from thermal decomposition of complex A11; (b) *In-situ* XRD patterns recorded for the thermal decomposition of A11 complex at different temperatures [* indicates peaks from sample holder]; (c) pattern for Pd_7Se_4 (from complex, A41) and (d) $PdSe_2$ along with $Pd_{17}Se_{15}$ obtained on thermal decomposition of complex, A14 at 250^oC for 1h in presence of N_2 (i), corresponding standard XRD pattern (ii).

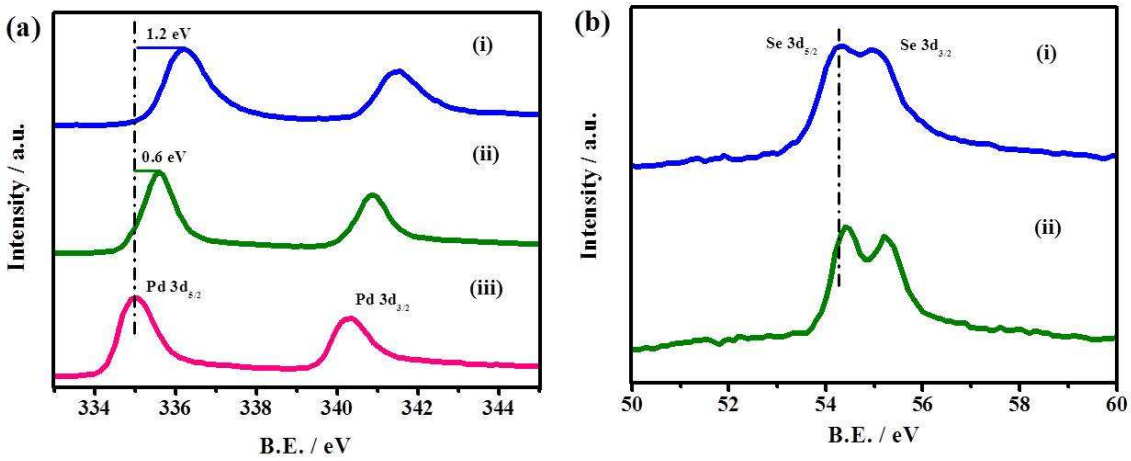

Figure 3. High resolution X ray photoelectron spectra of (a) Pd-3d and (b) Se-3d regions for $Pd_{17}Se_{15}$ (i), Pd_7Se_4 (ii) and Pd (iii) phases.

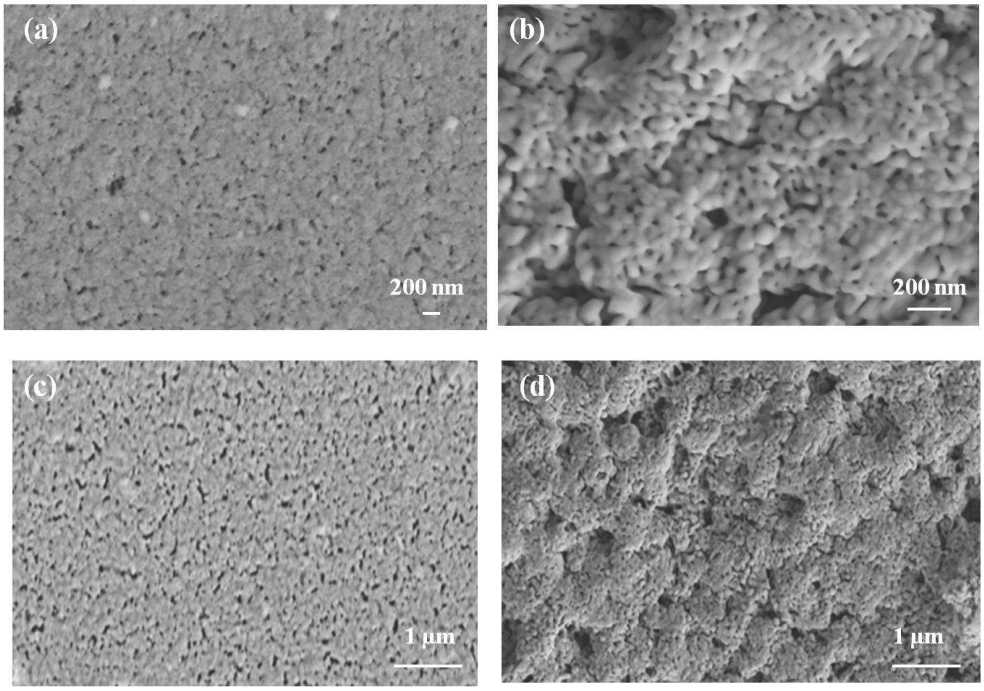

Figure 4. FESEM images at different magnifications of (a and c) $Pd_{17}Se_{15}$ and (b and d) Pd_7Se_4 phases obtained by thermolysis of the palladium seleno- complexes on FTO substrates.

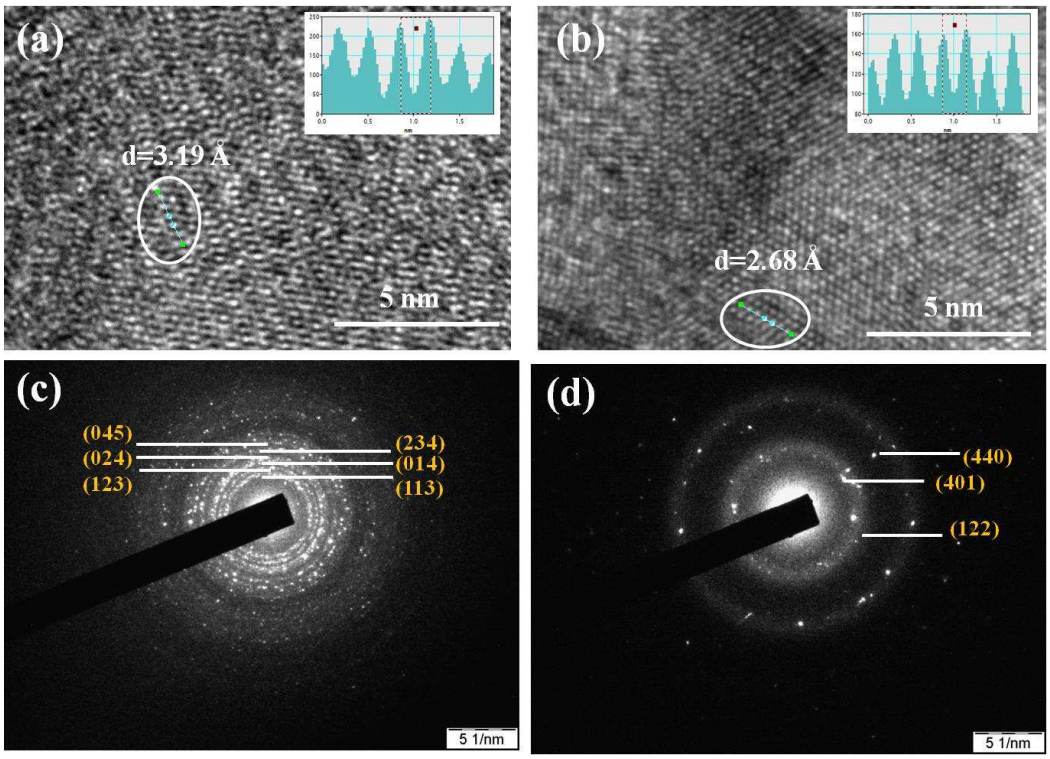

Figure 5. High resolution TEM images of (a) $Pd_{17}Se_{15}$ and (b) Pd_7Se_4 [inset shows the intensity line profile images of circular region] and (c) & (d) are selected area electron diffraction patterns of $Pd_{17}Se_{15}$ and Pd_7Se_4 respectively along with the corresponding crystallographic planes.

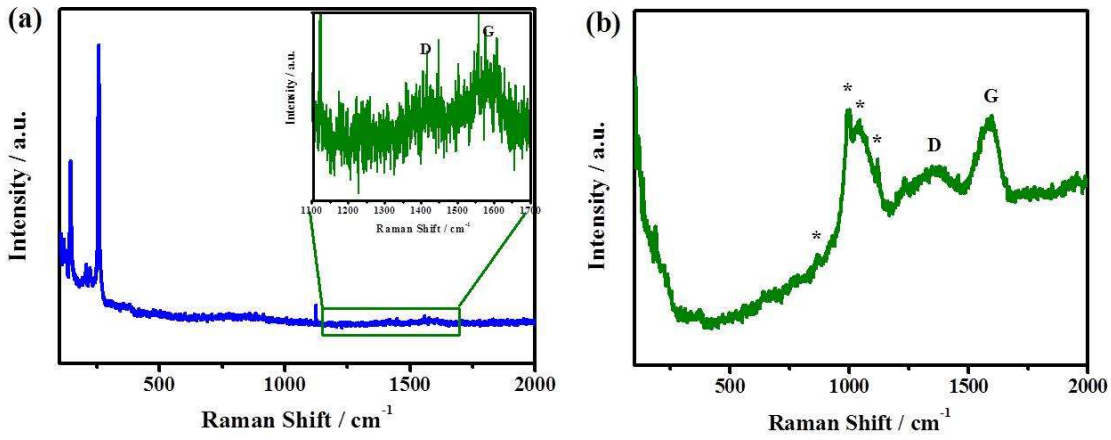

Figure 6. Raman spectrum of (a) $Pd_{17}Se_{15}$ film [inset shows the enlarged region from 1100 to 1700 cm^{-1}] and (b) Pd_7Se_4 film. Laser wavelength of 514 nm is used. [* represents bands from the glass slide].

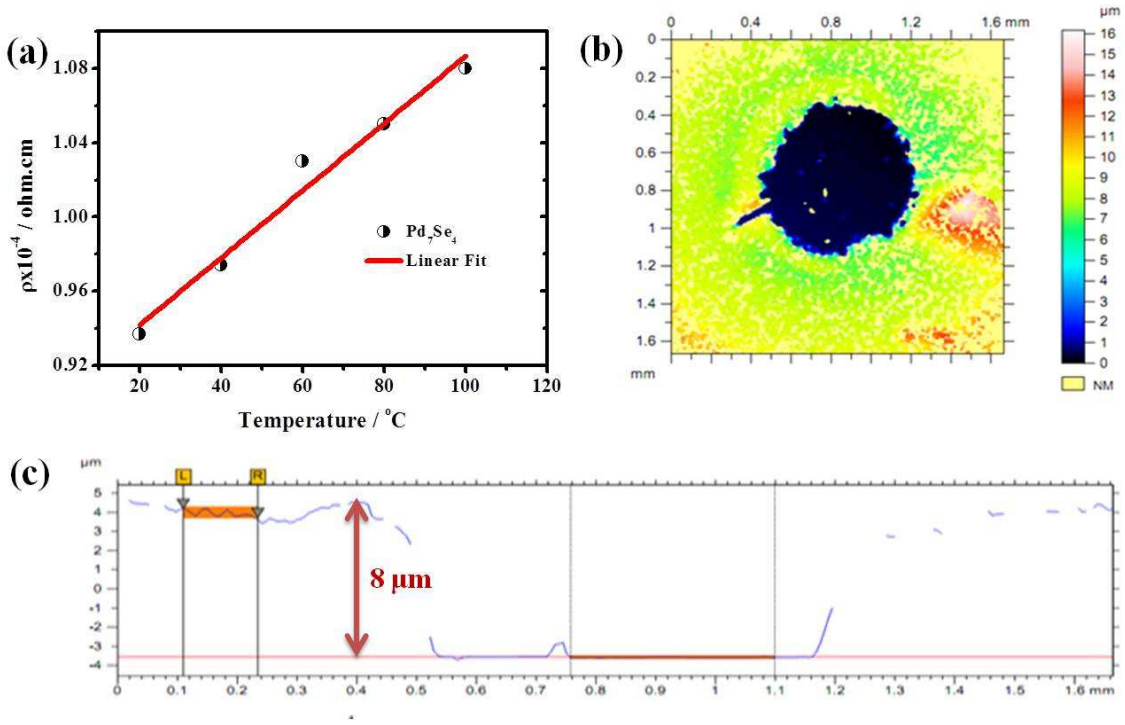

Figure 7. (a) Resistivity as a function of temperature, for Pd_7Se_4 film plotted on a linear scale; (b) Stylus profilometric measurements on Pd_7Se_4 film used for the resistivity measurements and (c) Line profile image of figure (b) where the film [shown as approximate circle in dark blue colour in (b)] shows a thickness of ~ 8 µm.

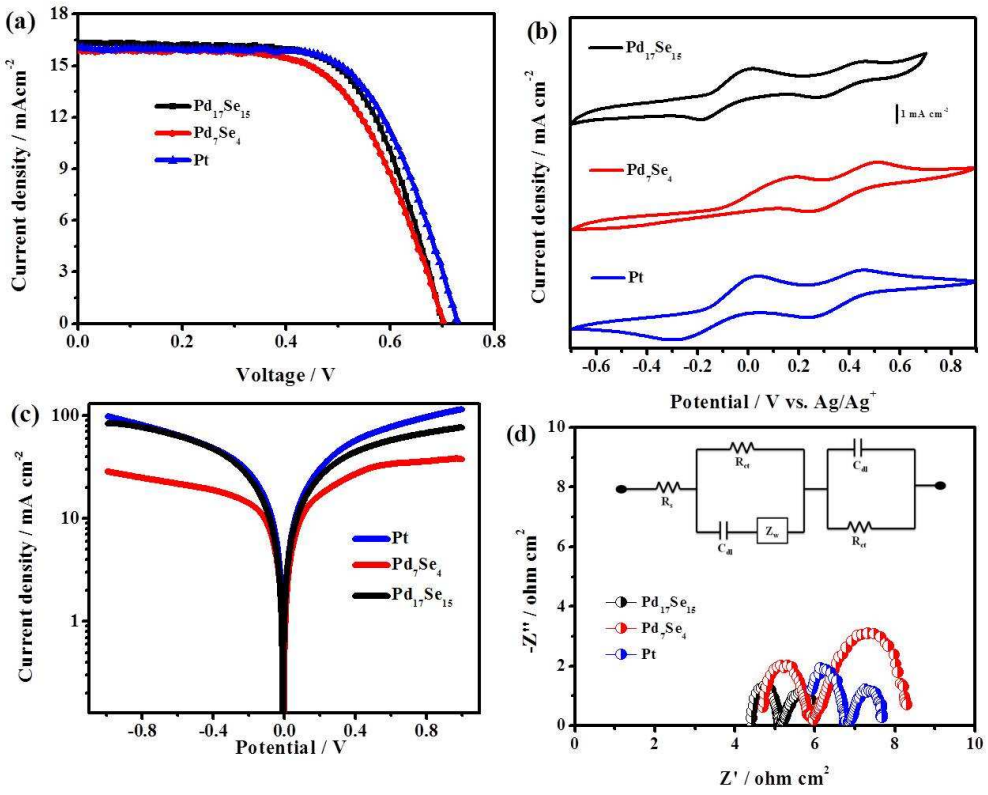

Figure 8. (a) Characteristic J-V curves of DSSCs with different counter electrodes, $Pd_{17}Se_{15}$ (black), Pd_7Se_4 (red) and Pt (blue); (b) corresponding cyclic voltammograms for $Pd_{17}Se_{15}$, Pd_7Se_4 and Pt; (c) Tafel polarization curves and (d) electrochemical impedance spectra for the two phases (inset shows the equivalent circuit used).

Table 1. Molar ratios of the precursors ($Pd(OAc)_2$: RSeSeR) used and the corresponding phases formed after thermal decomposition.

Mole ratio $Pd(OAc)_2$ **:RSeSeR**		**Phase formed**
1	1	$Pd_{17}Se_{15}$
2	1	Pd_7Se_4
3	1	Pd_7Se_4
4	1	Pd_7Se_4
1	2	$PdSe_2$ $Pd_{17}Se_{15}$
1	3	$PdSe_2$ $Pd_{17}Se_{15}$
1	4	$PdSe_2$ $Pd_{17}Se_{15}$

Table 2. (a) Binding energy values of Pd-3d peak and (b) Se-3d peak in different phases.

(a)

Material	Peak position (lower region) (eV)	Peak position (higher region) (eV)
$Pd_{17}Se_{15}$	336.2	341.4
Pd_7Se_4	335.5	340.5
Pd	335	340.2

(b)

Material	Lower region (eV)	Higher region (eV)
$Pd_{17}Se_{15}$	54.4	55.2
Pd_7Se_4	54.5	55.5

Table 3. Parameters of DSSCs with different counter electrodes and the simulated data from impedance spectra.

Solar cell parameters	**$Pd_{17}Se_{15}$**	**Pd_7Se_4**	**Pt**
J (mA cm^{-2})	16.32	15.85	16.02
V_{oc} (mV)	700	703	729
FF	0.65	0.61	0.65
Efficiency (%)	7.45	6.88	7.61
Impedance parameters			
R_s (Ω)	17.76	18.87	23.57
R_{ct} (Ω)	2.78	4.50	3.51
C_{dl} (µF)	0.30	0.14	0.16
W	0.25	0.13	0.22
Exchange current, ($mAcm^{-2}$)	11.5	9.5	13.5